

Mode areas and field energy distribution in honeycomb photonic bandgap fibers

Jesper Lægsgaard,¹ Niels Asger Mortensen,² and Anders Bjarklev¹

¹*Center for Communication, Optics and Materials (COM), Technical Univ. of
Denmark Bldg. 345v, DK-2800 Kgs. Lyngby, Denmark,*

²*Crystal Fibre A/S, Blokken 84, DK-3460 Birkerød, Denmark*

The field energy distributions and effective mode areas of silica-based photonic bandgap fibers with a honeycomb airhole structure in the cladding and an extra airhole defining the core are investigated. We present a generalization of the common effective area definition, suitable for the problem at hand, and compare the results for the photonic bandgap fibers with those of index-guiding microstructured fibers. While the majority of the field energy in the honeycomb photonic bandgap fibers is found to reside in the silica, a substantial fraction (up to $\sim 30\%$) can be located in the airholes. This property may show such fibers particularly interesting for sensor applications, especially those based on nonlinear effects or interaction with other structures (e.g. Bragg gratings) in the glass.

© 2018 Optical Society of America

OCIS codes: 060.2310 060.2370 060.2400 060.4370

1. Introduction

Photonic crystal fibers (PCFs), which guide light in a single-material structure by coherent scattering from an array of μm -sized airholes (for recent reviews we refer to Refs. 1, 2 and references therein), have in recent years emerged as an attractive alternative to conventional optical fibers within the area of nonlinear fiber devices.^{3,4} The advantages of the PCFs are firstly that very small mode areas can be obtained due to the large refractive index contrast between silica and air, leading to high nonlinearity coefficients. Secondly, the PCFs allow for a more flexible tailoring of the dispersion properties, which are crucial for many applications. PCFs with zero-dispersion wavelengths ranging from 565 to 1550 nm and high nonlinearity coefficients have been demonstrated.^{5,6}

The highly nonlinear PCFs fabricated today are of the index-guiding type,⁷ in which a missing hole in a triangular lattice of airholes defines a high-index core, which guides light by total internal reflection. Fibers guiding light in large hollow cores by means of the photonic band gap (PBG) effect have also been demonstrated,⁸ with the intention of obtaining very low losses and nonlinearities. However, an alternative PBG fiber design in which a honeycomb airhole lattice is modified by addition of an airhole to form a low-index core region⁹ has until now not been investigated thoroughly although its practical feasibility was demonstrated as early as 1998.¹⁰ The design is shown in Fig. 1, and can be characterised by three parameters: The physical distance between nearest-neighbor airholes (commonly denoted the pitch, or Λ), the diameter of the cladding holes, d_{cl} , and the diameter of the hole forming the core defect, d_c .

These fibers guide the majority of the light in silica, just as the conventional index-guiding PCFs, and may, therefore, constitute an alternative way of fabricating highly nonlinear fibers. The purpose of the present work is to investigate the design depicted in Fig. 1 with respect to field energy distribution and nonlinear coefficients. It will be shown that nonlinearities comparable to those obtained in index-guiding PCFs can be achieved in the honeycomb PBG fibers, while at the same time, a substantial fraction of the field energy may be pushed into the airholes. This may make these fibers particularly interesting for applications as sensing devices.^{11,12}

The rest of the paper is organized as follows: In Sect. 2, we describe our theoretical methods, and derive a generalized formula for the fiber nonlinearity coefficient, in terms of an effective area, which is valid for all field distributions, including those where a substantial part of the field energy resides in air. In Sect. 3, we present and discuss our numerical results for some selected honeycomb designs, and compare them to results for index-guiding PCFs. Finally, Sect. 4 summarizes our conclusions.

2. Theoretical approach

We consider a structure, which is uniform along the z -axis while structured in the x - y plane. The magnetic field vector, \mathbf{H} , may then be written:

$$\mathbf{H}(\mathbf{r}) = e^{i(\omega t - \beta z)} \mathbf{H}(x, y), \quad (1)$$

for a monochromatic wave. The fundamental equation for \mathbf{H} is:

$$\frac{\omega^2}{c^2} = \frac{\langle \mathbf{H}, \Theta \mathbf{H} \rangle}{\langle \mathbf{H}, \mathbf{H} \rangle}, \quad (2)$$

$$\Theta \mathbf{H} = \nabla \times \frac{1}{\epsilon_r(\mathbf{r})} \nabla \times \mathbf{H} \quad (3)$$

where $\varepsilon(\mathbf{r}) = \varepsilon_0 \varepsilon_r(\mathbf{r})$ is the dielectric function. For a fixed propagation constant, β , this equation may be solved for ω , which can then be regarded as a function of β and $\varepsilon(\mathbf{r})$. From the magnetic field vector, the corresponding electric field is straightforwardly obtained using Amperes law (SI units are used throughout the paper):

$$\nabla \times \mathbf{H} = i\omega\varepsilon\mathbf{E} \quad (4)$$

The effective area is a concept originating in the theory of third-order nonlinearity effects in optical waveguides.¹³ In a homogeneous material, such as amorphous silica, the third-order part of the nonlinear susceptibility gives rise to an amplitude dependent shift in the material refractive index:

$$n = n_0 + \Delta n = n_1 + n_2 |\mathbf{E}|^2 \quad (5)$$

where n_1 is the refractive index of silica in the limit of zero field, and n_2 is a nonlinear coefficient related to the nonlinear-susceptibility tensor, $\chi^{(3)}$, through:¹³

$$n_2 = \frac{3}{8n_1} \text{Re}\chi_{xxxx}^{(3)}. \quad (6)$$

In an optical fiber, the change in material index leads to a corresponding change in the effective index ($n_{\text{eff}} = \frac{\beta}{\omega}$). In first-order perturbation theory, the mode-field distribution can be considered unchanged by the index perturbation, and the change in ω for a (Kerr-induced) $\Delta\varepsilon$ for fixed β is from Eq. (2) found to be:

$$\Delta\omega = -\frac{\omega\varepsilon_0 c^2 \langle \mathbf{E}, \Delta\varepsilon_r \mathbf{E} \rangle}{2 \langle \mathbf{H}, \mathbf{H} \rangle}. \quad (7)$$

Usually, the experimental situation is that light is launched at a fixed frequency ω_0 and the Kerr-induced change in refractive index effects a change in the propagation constant β from β_0 , say, to $\beta_0 + \Delta\beta$. $\Delta\beta$ is then determined by:

$$\omega(\beta_0 + \Delta\beta) + \Delta\omega = \omega_0, \quad \omega(\beta_0) = \omega_0. \quad (8)$$

Here, $\omega(\beta)$ is the relation between ω and β in the absence of the Kerr effect, and we have neglected the change in $\Delta\omega$ arising from the shift in β , assuming that both $\Delta\omega$ and $\Delta\beta$ are small. We can then obtain $\Delta\beta$ by linear expansion:

$$\frac{\partial\omega}{\partial\beta}\Delta\beta = -\Delta\omega \Rightarrow \Delta\beta = -\frac{\Delta\omega}{v_g^0} \quad (9)$$

Here, v_g^0 is the waveguide group velocity in the absence of material dispersion effects (since we consider propagation at a fixed frequency, the frequency dependence of ε should not be taken into account when evaluating $\frac{\partial\omega}{\partial\beta}$). The change in n_{eff} arising from the Kerr effect is then:

$$\Delta n_{\text{eff}} = -\frac{c\Delta\omega}{v_g^0\omega_0}. \quad (10)$$

For $\Delta\varepsilon_r$ we have:

$$\Delta\varepsilon_r = 2\sqrt{\varepsilon_r}n_2 |\mathbf{E}|^2 + O(n_2^2|\mathbf{E}|^4), \quad (11)$$

and thereby, neglecting the small $n_2^2 |\mathbf{E}|^4$ term and using $\sqrt{\varepsilon_r} = n_1$:

$$\Delta n_{\text{eff}} = \frac{\varepsilon_0 c^3 \int n_1 n_2 |\mathbf{E}|^4 dA}{v_g^0 \langle \mathbf{H}, \mathbf{H} \rangle} = \frac{\varepsilon_0 c \int n_1 n_2 |\mathbf{E}|^4 dA}{v_g^0 \langle \mathbf{E}, \mathbf{D} \rangle} \quad (12)$$

where, in the last equality, the inner product of \mathbf{H} with itself has been rewritten using Eq. (2) and (4). The integral is taken over the xy -plane. Note that, for a microstructured fiber, n_1, n_2 are position-dependent quantities.

In the case of ordinary silica fibers, the parameters n_1, n_2 have little variation over the fiber cross section, and it is common practice to express the Kerr-induced change in the guided-mode effective index as:

$$\Delta n_{\text{eff}} = P \frac{n_2^P}{A_{\text{eff}}} \quad (13)$$

where P is the power launched into the fiber, $n_2^P = \frac{n_2}{n_1 \varepsilon_0 c}$ and A_{eff} is the effective mode area. In a microstructured fiber, both n_1 and n_2 can have a strong position dependence, and a generalization of Eq. (13) is not straightforward. However, in the case where n_1, n_2 are piecewise constant functions, taking on N different values over the fiber cross section, we can modify the above definition to:

$$\Delta n_{\text{eff}} = P \sum_{i=1}^N \frac{n_{2i}^P}{A_{\text{eff}}^i} \quad (14)$$

where n_{2i}^P denote the value of n_2^P in the different sections of the fiber. It can be shown¹⁴ that P and v_g^0 are connected by:

$$P = \int (\mathbf{E} \times \mathbf{H})_z dA = v_g^0 \langle \mathbf{E}, \mathbf{D} \rangle \quad (15)$$

From Eqs. (12),(15) we now obtain:

$$\Delta n_{\text{eff}} = P \sum_{i=1}^N n_{2i}^P \frac{(n_1^i \varepsilon_0 c)^2 \int_i |\mathbf{E}|^4 dA}{(v_g^0 \langle \mathbf{E}, \mathbf{D} \rangle)^2} = P \sum_{i=1}^N n_{2i}^P \frac{(n_1^i n_g^0)^2 \int_i |\mathbf{E}|^4 dA}{\langle \mathbf{E}, \mathbf{D}_r \rangle^2} \quad (16)$$

In the last step, we have introduced $\mathbf{D}_r = \varepsilon_r \mathbf{E}$ and the effective group index of the guided mode, $n_g^0 = \frac{c}{v_g}$. Note that the integral over $|\mathbf{E}|^4$ in each term is restricted to the regions with $n_1 = n_1^i$. Comparing Eqs. (14) and (16), it can be seen that:

$$\begin{aligned} A_{\text{eff}}^i &= \frac{\langle \mathbf{E}, \mathbf{D}_r \rangle^2}{(n_1^i n_g^0)^2 \int_i |\mathbf{E}|^4 dA} \\ &= \left(\frac{n_1^i}{n_g^0} \right)^2 \frac{\langle \mathbf{E}, \mathbf{D}_r \rangle^2}{\int_i |\mathbf{E} \cdot \mathbf{D}_r|^2 dA} \end{aligned} \quad (17)$$

In the present paper, we shall only be concerned with the case of pure silica/air fibers, in which n_1, n_2 are equal to 1 and 0, respectively, in the air regions while having the values appropriate for silica in the rest of the transverse plane. In this case, the nonlinear coefficient will be entirely determined by the effective area relating to the silica regions, that is:

$$A_{\text{eff}} = \left(\frac{n_1}{n_g^0} \right)^2 \frac{\langle \mathbf{E}, \mathbf{D}_r \rangle^2}{\int_{\text{SiO}_2} |\mathbf{E} \cdot \mathbf{D}_r|^2 dA} \quad (18)$$

The values for n_1, n_2 are now understood to be those of pure silica.

At this point, two comments are in order: Firstly, note that of the two n_1 factors in the denominator of Eq. (18), one comes from the definition of n_2^P in terms of n_2 , whereas the other one comes from the fundamental wave equation. Therefore, if one uses a table value of n_2^P derived with a n_1 different from that at which experiments are done, it may be necessary to use two different n_1 values in the product. Secondly, Eq. (18) differs somewhat from the formula commonly used for A_{eff} , namely:

$$\tilde{A}_{\text{eff}} = \frac{(\int |\mathbf{E}|^2 dA)^2}{\int |\mathbf{E}|^4 dA} \quad (19)$$

However, if we assume that all the field energy resides in the silica regions of the fiber, and that $n_g^0 \approx n_1$ we obtain:

$$\left(\frac{n_1}{n_g^0}\right)^2 \frac{\langle \mathbf{E}, \mathbf{D}_r \rangle^2}{\int_{\text{SiO}_2} |\mathbf{E} \cdot \mathbf{D}_r|^2 dA} = \frac{(\int n_1^2 |\mathbf{E}|^2 dA)^2}{(n_1 n_g^0)^2 \int |\mathbf{E}|^4 dA} \approx \frac{(\int |\mathbf{E}|^2 dA)^2}{\int |\mathbf{E}|^4 dA} \quad (20)$$

Thus, the commonly used formula (19) appears as a limiting case of the more general result (18). The approximations leading from Eq. (18) to (19) are reasonably well fulfilled in standard fibers and in most index-guiding PCFs. This is, however, not the case for the fiber designs examined in the present work. In Fig. 2 we show the relative difference between the A_{eff} definitions in Eqs. (18),(19) defined as:

$$\Delta A_{\text{eff}} = A_{\text{eff}} - \tilde{A}_{\text{eff}} \quad (21)$$

with A_{eff} , \tilde{A}_{eff} given by Eqs. (18), (19) respectively. The differences have been calculated for some fibers designed to have a substantial part of the field energy in air, as discussed in the next section. It is evident that differences of 10-20% between the two definitions can easily occur. Also, the difference varies in both sign and magnitude over the transmission window of the fibers, so that no simple scaling rule between the two definitions can be extracted.

In this work, we solve Eq. (2) by expanding the magnetic field and the dielectric function in plane waves, using a freely available software package.¹⁵ Eq. (4) can be used to derive the electric field vector from the magnetic, and the effective area can then be found from Eq. (18). Since it is important for many applications of nonlinear effects to be close to a wavelength at which the group velocity dispersion is zero,

we have also investigated the dispersion properties of the fibers. In order to scan a range of physical pitches efficiently we have used a recently developed perturbative approach to the inclusion of material dispersion effects.¹⁶ We have found this scheme to be both efficient and accurate in the case of silica/air microstructured fibers.

3. Numerical results and discussion

In the present investigation, we will primarily focus on structures with $\frac{d}{\Lambda}$ lying in the interval between 0.3 and 0.8 for both core and cladding holes. Such structures are by now routinely fabricated by fusing and drawing hand-stacked capillary tubes and rods of silica. However, in order to investigate the limitations of the hole-defect honeycomb PBG fibers, we have also studied a design with $\frac{d_{cl}}{\Lambda}=0.95$ and $\frac{d_c}{\Lambda}$ in the range between 0.1 and 0.3. Results for $\frac{d_c}{\Lambda}=0.1, 0.2$ and 0.3 are shown in Fig. 3. The lowest value of A_{eff} is $0.76\lambda^2$ and is obtained for $\frac{d_c}{\Lambda}=0.2$. The occurrence of a minimum A_{eff} as a function of core hole diameter can be understood as follows: Since nonlinear effects only occur in the silica part of the fiber, reduction of core hole size increase the region of integration in the denominator of Eq. (18), thereby acting to decrease the effective area. On the other hand, as is evident from Fig. 3, reduction of the core hole size also decreases the values of $\frac{\lambda}{\Lambda}$, where the guided mode becomes localized. In other words, the fiber dimensions becomes larger relative to the wavelength of the guided mode, and this acts to increase the effective area, when measured relative to λ^2 .

In the case of index-guiding PCFs, effective areas as low as $1.7 \mu\text{m}^2$ at a wavelength of $1.55 \mu\text{m}$ have been reported experimentally, corresponding to $A_{\text{eff}} \sim 0.75\lambda^2$.

The minimal mode area that can be obtained in a silica rod in air has been proposed as a theoretical lower limit on the effective area in silica-based index-guiding fibers, and has been found to be $1.48 \mu\text{m}^2$ at $1.55 \mu\text{m}$ (or $0.62\lambda^2$).¹⁷ Thus, in spite of the fact that the guided mode is localized around an airhole in the honeycomb structures considered here they are able to obtain mode areas, which are only slightly larger than what is possible in index-guiding PCFs.

In Fig. 4 we show the effective area as a function of wavelength for $\frac{d_{cl}}{\Lambda}=0.56$, 0.68 and 0.80, and $\frac{d_c}{\Lambda}$ around 0.3-0.5. It can be seen that $A_{\text{eff}} \sim 1.5 - 3\lambda^2$ is readily obtained, and that the minimal area decreases with increasing size of the cladding holes and increases for increasing size of the core hole.

In many experiments involving nonlinear effects it is important to work at a wavelength at which the chromatic dispersion of the fiber is close to zero. In these situations, it is the minimal effective area obtainable at a given wavelength, under the condition that the dispersion coefficient be zero, which is of interest. Both index- and PBG-guiding PCFs can have complicated dispersion curves with several zero-dispersion points. Some examples of what can be achieved with the honeycomb design for $\frac{d_{cl}}{\Lambda}=0.68$ are shown in Fig. 5. Following the three curves with $d_c/d_{cl}=0.45$ it can be seen that the zero-dispersion point can have a discontinuous behaviour as a function of Λ . The curve for $d_c/d_{cl}=0.55$ is an example of a fiber with several dispersion zeros. To investigate the effective area at the zero-dispersion point we have chosen to focus on the longest zero-dispersion wavelength for a given design, since this is where one will usually have the smallest effective area relative to the wavelength of the light. For the PBG fiber we have, therefore, investigated the location of the longest zero-

dispersion wavelength, λ_0 over a range of physical fiber dimensions from $\sqrt{3}\Lambda=1.5$ to $5 \mu\text{m}$. In Fig. 6 we report λ_0 versus the physical pitch, Λ , and in Fig. 7 the effective area at λ_0 is plotted versus λ_0 . Broken curves indicate a discontinuity in λ_0 as a function of Λ . In some cases, the zero-dispersion wavelength can sweep over the same frequency several times as Λ is varied, which is why some of the curves in Fig. 7 are multi-valued. Generally, the honeycomb fibers tend to have dispersion zeros falling in the range between 0.8 and $2 \mu\text{m}$.

For comparison we have also considered index-guiding PCFs with a triangular array of airholes constituting the cladding and a core-defect formed by a missing air hole. For air hole diameters $d \leq d^*$ (with $d^* \sim 0.45\Lambda$) this class of PCFs is endlessly single mode⁷ and by scaling the pitch both large-mode area PCFs as well as small-core non-linear PCFs can be formed. In addition to the mode-size the dispersion properties may also be engineered. In the top panel of Fig. 8 we show the zero-dispersion wavelength λ_0 as a function of the pitch Λ for 5 hole diameters. Depending on the pitch the PCF may have none, one, or two (or even three if also considering the near-infrared regime) dispersion zeros. For the situation with two dispersion zeros it is seen that the second dispersion zero (counting from the short wavelength limit) depends strongly on both the pitch and the hole diameter whereas for the first dispersion zero the dependence on hole diameter dominates over the much weaker dependence on pitch. One of the exciting properties of these PCFs is that by increasing the hole diameter the lowest dispersion zero can be moved toward the visible regime. In the lower panel of Fig. 8 we show the effective area versus zero-dispersion wavelength. In general we find that when the hole size is increased the mode becomes more tightly confined

with a smaller effective area. The plot also illustrates a highly desired property; when shifting the first dispersion-zero toward the visible the effective area also decreases so that the intensity thresholds for various non-linear phenomena also decreases. We note that the first dispersion zero may be moved to the visible and the effective area may be decreased by further increasing the air hole diameter (so that $d > d^*$), but then care must be taken that the PCF remain single-mode near the dispersion zero.

Comparing Figs. 7 and 8 it can be seen that the honeycomb PBG fibers investigated here do not offer substantially improved flexibility in the tailoring of mode areas and dispersion properties compared to the index-guiding PCFs. The PBG designs with large cladding holes do seem to offer smaller mode areas at the longer values of λ_0 but this could also be obtained in index-guiding PCFs by increasing the size of the airholes, thereby going further out of the endlessly single-mode regime. Determining the single-mode regime for PBG fibers with large cladding airholes is difficult due to the appearance of multiple bandgaps even at relatively long values of $\frac{\lambda}{\Lambda}$. For the fibers with $\frac{d_{cl}}{\Lambda}=0.8$ we have found that a guided second-order mode is present at λ_0 over most of the Λ range investigated. For the fibers with smaller values of $\frac{d_{cl}}{\Lambda}$ the second-order modes mostly appears at wavelengths shorter than λ_0 for Λ -values smaller than $\sim 2 \mu\text{m}$ meaning that a useful range of λ_0 values without second-order mode guidance is available. We have not, however, checked for the presence of guided modes in higher-order gaps.

One interesting feature of the honeycomb PBG design compared to the index-guiding PCFs is that a relatively large fraction of the field energy resides in the airholes of the fiber. This is illustrated in Fig. 9, where the fraction of electric field energy

present in air has been plotted for the fiber designs discussed above. It is evident that energy fractions of 10-15% in air are readily obtained, even for holes of moderate size, and that the fraction increases with increasing size of the core hole defect. To estimate the range of energy distributions accessible, we have investigated some designs, in which the core hole defect has been further enlarged. In Fig. 10, we show results for effective areas and the energy fraction in air for fibers with $\frac{d_c}{\Lambda}$ around 0.6 and varying size of the cladding holes. It can be seen that the energy fraction in air can be as large as 30%, while still having a range of possible zero-dispersion wavelengths and fairly small mode areas. Further increase of d_c does not push appreciably more field energy into the airholes, however, the transmission windows and accessible zero-dispersion ranges are quickly diminished. The somewhat counterintuitive fact that the minimum of the effective area curves (i.e., the maximum of the nonlinear coefficient at a particular wavelength) occurs approximately at the same $\frac{\lambda}{\Lambda}$ values as the maximum of the energy fraction in the airholes is due to the fact that the energy fraction in air is high at long wavelengths, where the fiber size relative to wavelength is small.

In Fig. 11 we show some radial mode profiles obtained by integrating the electric field energy density over the angular coordinate in a polar coordinate system around the core center. The curves are calculated for fibers with $\frac{d_{cl}}{\Lambda} = 0.8$ and varying size of the core hole, and have been normalized so that their radial integral is unity. The wavelength has been chosen so as to maximize the fraction of field energy in air. Only 5-10% of the field energy is present in the central hole defining the core. This shows that the increase in the energy fraction present in air for increasing $\frac{d_c}{\Lambda}$ is not so much due to the field energy being pushed into the central core hole, but rather

to an increase of the field energy present in the cladding region as is also evident from Fig. 11. The presence of a substantial part of the field energy in air not only influences the integrals in Eq. (18), but also makes the group velocity of the guided mode deviate substantially from the material refractive index, thus influencing the prefactor $\left(\frac{n_+}{n_g}\right)^2$. In Fig. 12, this fraction is depicted for the designs with $\frac{d_{cl}}{\Lambda}=0.8$. Its importance for a correct evaluation of the effective area in these structures is evident.

The power fraction in air (which is not completely equivalent to the quantity calculated here) for index-guiding PCFs was investigated by Monro and co-workers¹⁸ who found that large airhole diameters and $\frac{\lambda}{\Lambda}$ -values were needed to obtain appreciable power fractions in air. In Fig. 13, we report the fraction of field energy in air for some index-guiding PCFs with the same cladding structure as those discussed above but somewhat larger airholes. Comparing Figs. 9 and 10 with Fig. 13 it is evident that the λ/Λ values needed to push a given fraction of field energy into the air region are considerably larger in the index-guiding fibers, calling for smaller values of the physical pitch for operation at a given wavelength. This may make the honeycomb fibers particularly relevant for evanescent field devices,^{11,12} such as gas sensors, based on interactions with the glass, through, e.g., nonlinear effects or inscribed Bragg gratings.

4. Conclusion

In conclusion, we have investigated the field energy distribution and nonlinear coefficients of honeycomb photonic bandgap fibers and compared them to index-guiding photonic crystal fibers with a cladding structure consisting of a triangular array of

airholes. A generalized concept of effective mode area, which is adequate for the treatment of fibers with a substantial part of the field energy present in the airholes, has been derived for this purpose. While the honeycomb fibers do not seem to offer increased flexibility in the design of dispersion properties and mode areas they do offer the same possibilities as the index-guiding fibers, at wavelengths above $\sim 1 \mu\text{m}$. In addition, the honeycomb fibers have a larger fraction of the field energy present in the airholes which may make these fibers particularly interesting for sensor applications based on interactions with the glass, through e.g. nonlinear effects and/or inscribed Bragg gratings.

References

1. J. C. Knight and P. St. J. Russell. Applied optics: New ways to guide light. *Science*, 296:276–277, 2002.
2. T. A. Birks, J. C. Knight, B. J. Mangan, and P. St. J. Russell. Photonic crystal fibres: An endless variety. *IEICE Trans. Electron.*, E84-C:585–591, 2001.
3. N. G. R. Broderick, T. M. Monro, P. J. Bennett, and D. J. Richardson. Nonlinearity in holey optical fibers: measurement and future opportunities. *Opt. Lett.*, 24:1395–97, 1999.
4. J. K. Ranka, R. S. Windeler, and A. J. Stentz. Visible continuum generation in air-silica microstructure optical fibers with anomalous dispersion at 800 nm. *Opt. Lett.*, 25:25–27, 2000.
5. J. C. Knight, J. Arriaga, T. A. Birks, A. Ortigosa-Blanch, W. J. Wadsworth, and P. St. J. Russell. Anomalous dispersion in photonic crystal fiber. *IEEE Photonic*

- Tech. L.*, 12:807–809, 2000.
6. K. P. Hansen, J. R. Jensen, C. Jacobsen, H. R. Simonsen, J. Broeng, P. M. W. Skovgaard, and A. Petersson. Highly nonlinear photonic crystal fiber with zero-dispersion at 1.55 μm , OFC 2002 post deadline paper FA9.
 7. J. C. Knight, T. A. Birks, P. St. J. Russell, and D. M. Atkin. All-silica single-mode optical fiber with photonic crystal cladding. *Opt. Lett.*, 21:1547–1549, 1996.
 8. R. F. Cregan, B. J. Mangan, J. C. Knight, T. A. Birks, P. St. J. Russell, P. J. Roberts, and D. C. Allan. Single-mode photonic band gap guidance of light in air. *Science*, 285:1537–1539, 1999.
 9. J. Broeng, S. E. Barkou, A. Bjarklev, J. C. Knight, T. A. Birks, and P. S. J. Russell. Highly increased photonic band gaps in silica/air structures. *Opt. Commun.*, 156:240–244, 1998.
 10. J. C. Knight, J. Broeng, T. A. Birks, and P. St. J. Russell. Photonic band gap guidance in optical fibers. *Science*, 282:1476–1478, 1998.
 11. T. M. Monro, W. Belardi, K. Furusawa, J. C. Baggett, N. G. R. Broderick, and D. J. Richardson. Sensing with microstructured optical fibres. *Meas. Sci. Technol.*, 12:854–8, 2001.
 12. Y. L. Hoo, W. Jin, H. L. Ho, D. N. Wang, and R. S. Windeler. Evanescent-wave gas sensing using microstructure fiber. *Opt. Eng.*, 41:8–9, 2002.
 13. G. P. Agrawal. *Nonlinear Fiber Optics*. Academic Press, San Diego, 2001.
 14. A. W. Snyder and J. D. Love. *Optical Waveguide Theory*. Chapman & Hall, London, 1996.

15. S. G. Johnson and J. D. Joannopoulos. Block-iterative frequency-domain methods for Maxwell's equations in a planewave basis. *Opt. Express*, 8:173–190, 2001.
16. J. Lægsgaard, S. E. B. Libori, and A. Bjarklev. Chromatic dispersion in photonic crystal fibers: Fast and accurate scheme for calculation. *J. Opt. Soc. Am. B*, 20:in press, 2003.
17. T. A. Birks, D. Mogilevtsev, J. C. Knight, and P. S. J. Russell. Dispersion compensation using single-material fibers. *IEEE Photon. Tech. Lett.*, 11:674–676, 1999.
18. T. M. Monro, D. J. Richardson, and P. J. Bennett. Developing holey fibres for evanescent field devices. *Electronics Letters*, 35:1189–89, 1999.

List of Figure Captions

Fig. 1 The generic PCF structure investigated in the present work. The core and innermost cladding holes are shown along with the defining parameters d_c , d_{cl} , and Λ .

Fig. 2 Relative difference between the effective area definition proposed here, Eq. (18), and the commonly used definition, Eq. (19).

Fig. 3 Effective area, relative to wavelength, calculated from Eq. (18) for a fiber with $\frac{d_{cl}}{\Lambda}=0.95$ and various values of the core hole diameter, d_c .

Fig. 4 Effective area relative to the wavelength of the guided mode for honeycomb PBG fibers with $\frac{d_{cl}}{\Lambda}=0.56$ (a), 0.68 (b) and 0.8 (c) and various values of $\frac{d_c}{d_{cl}}$.

Fig. 5 Plots of the chromatic dispersion coefficient, D , in units of ps/nm/km for various values of the pitch in a honeycomb PBG fiber with $\frac{d_{cl}}{\Lambda}=0.68$ and $\frac{d_c}{d_{cl}}=0.45$.

Fig. 6 Longest zero-dispersion wavelength, λ_0 , as a function of the physical pitch, Λ . Structures and labeling as in Fig. 4.

Fig. 7 Effective area at the zero-dispersion wavelength, λ_0 as a function of λ_0 . Structures and labeling as in Fig. 4.

Fig. 8 Effective area and dispersion zeros for index-guiding PCFs. Top panel: Zero-dispersion wavelength versus pitch. Lower panel: Effective area at the zero-dispersion wavelength as a function of the zero-dispersion wavelength.

Fig. 9 The fraction of the electric field energy of the guided mode present in the airholes. Structures and labeling as in Fig. 4.

Fig. 10 Effective area relative to wavelength (a), effective area at the zero-

dispersion wavelength (b) and energy fraction in air (c) for some fiber designs in which a substantial part of the field energy resides in the airholes.

Fig. 11 Radial profile of the electric field energy density, obtained by integration over the angular coordinate in a coordinate system with origin at the core center. The curves are normalized to have unit radial integrals. The thin vertical lines indicate the position of the first ring of cladding airholes.

Fig. 12 Variation of the prefactor $\frac{n_1}{n_g^0}$ in Eq. (18) with wavelength for a fiber with $\frac{d_{cl}}{\Lambda}=0.8$ and various values of the core hole diameter, d_c .

Fig. 13 Energy fraction in air of index guiding fibers with a cladding structure as shown in Fig. 8 and various airhole diameters d .

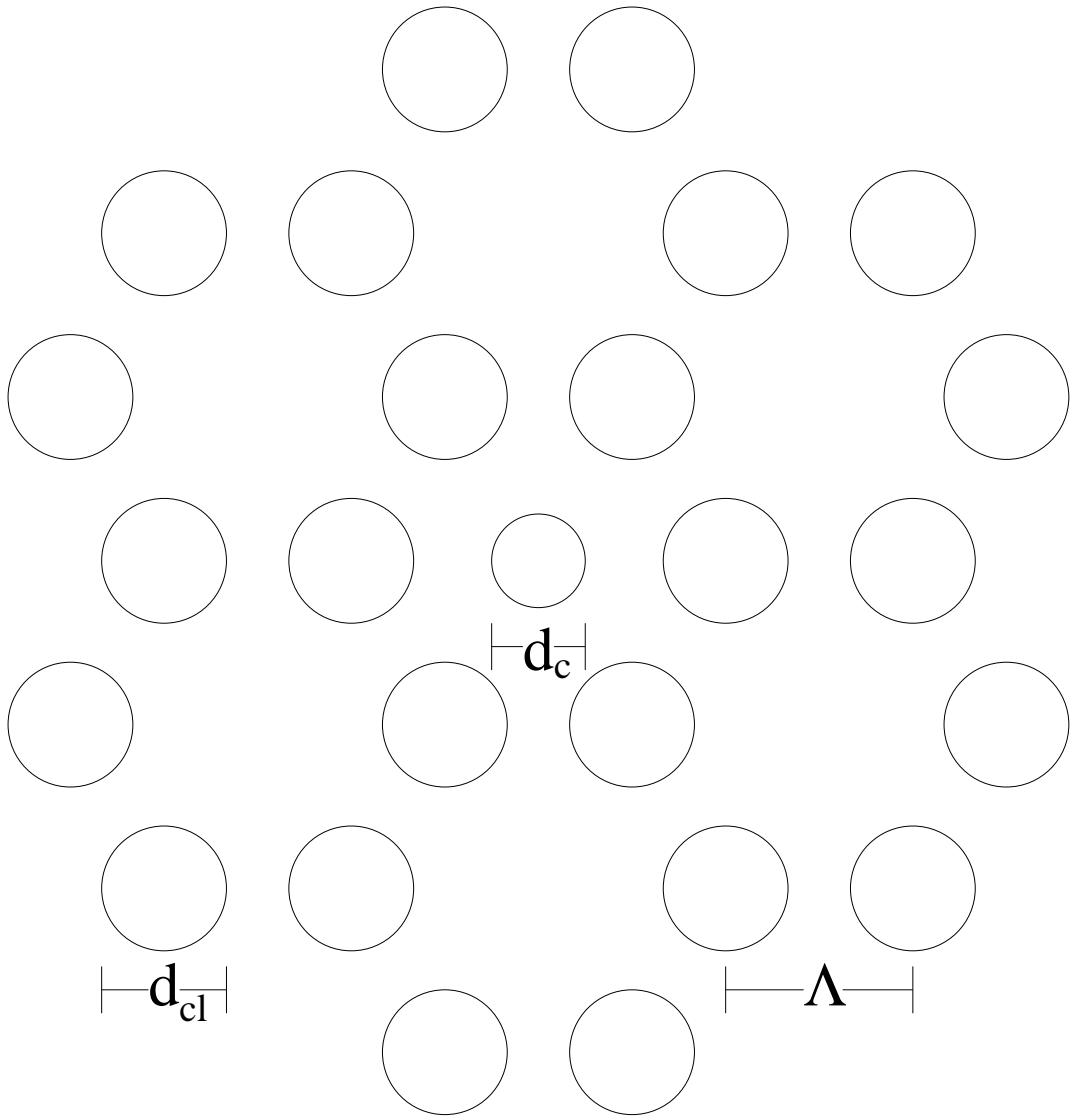


Fig. 1. LÆGSGAARD

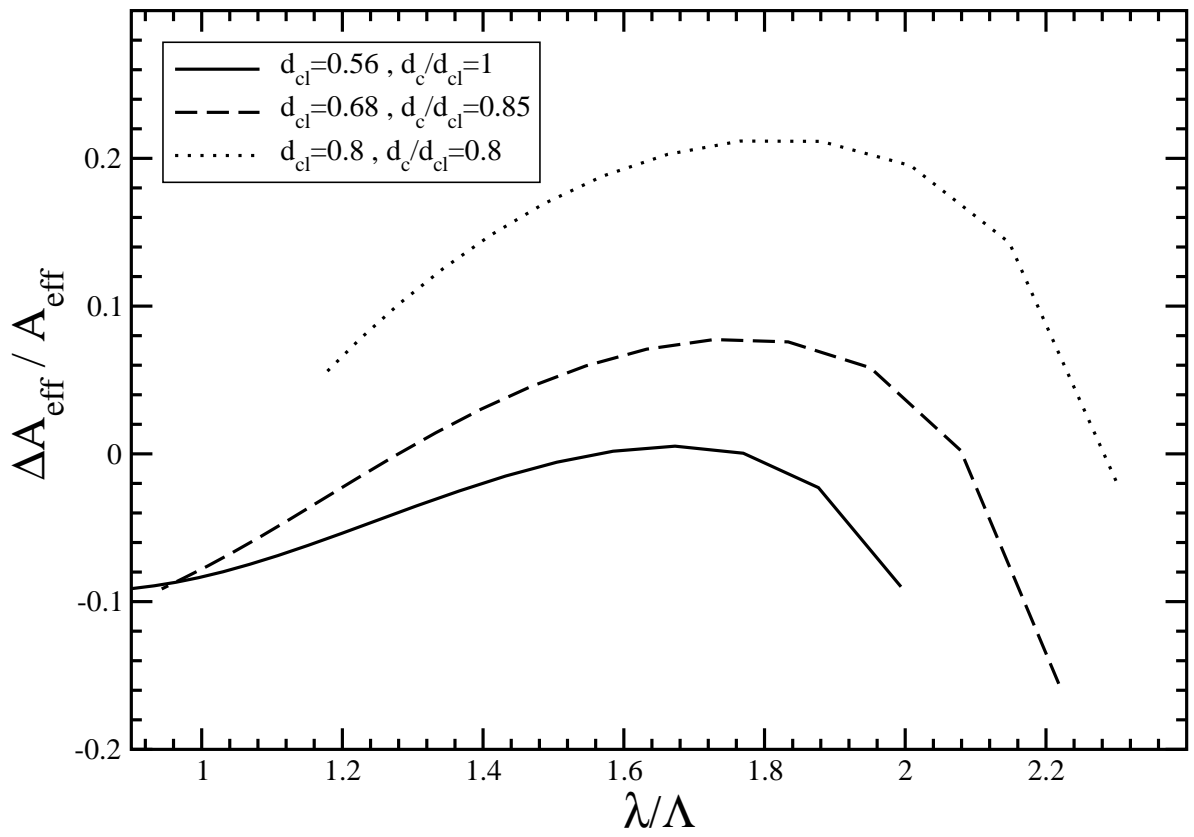


Fig. 2. LÆGSGAARD

$d_{cl}/\Lambda=0.95$

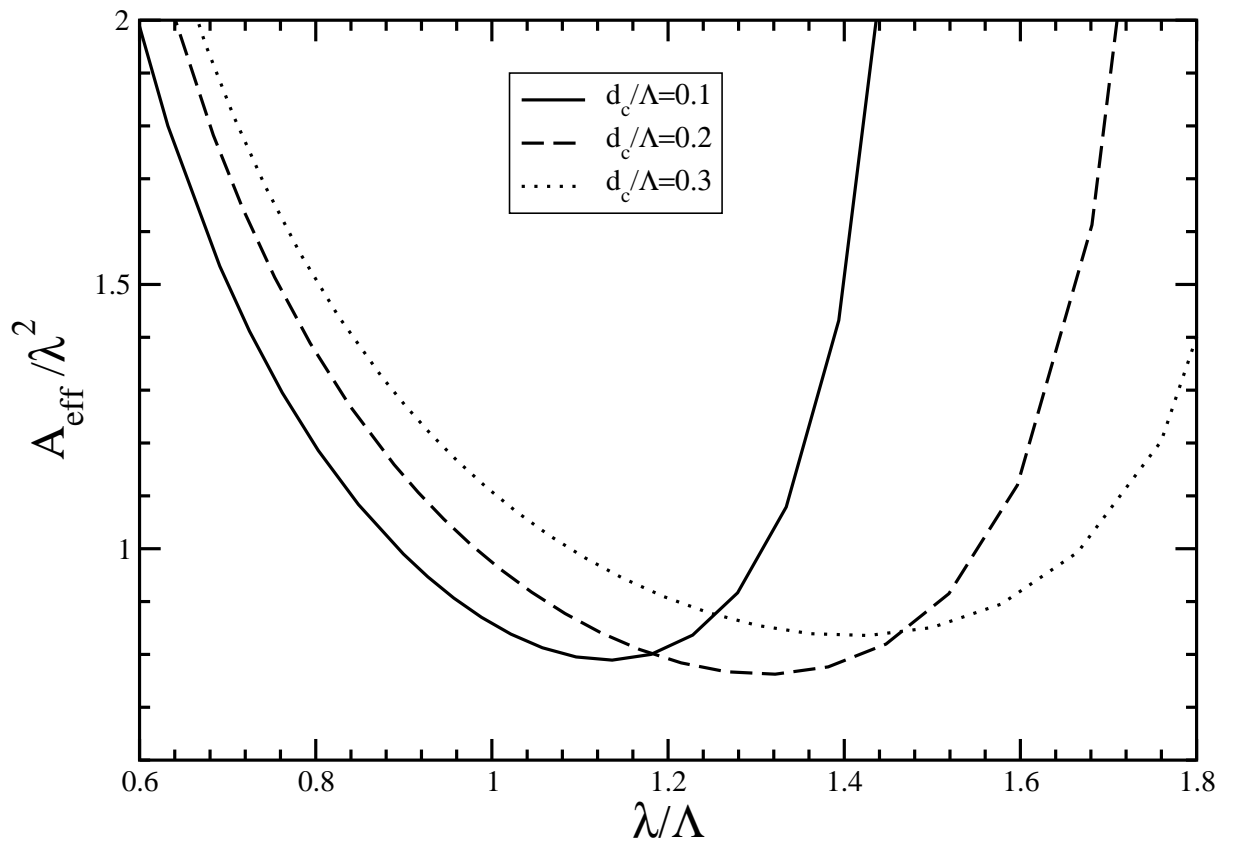


Fig. 3. LÆGSGAARD

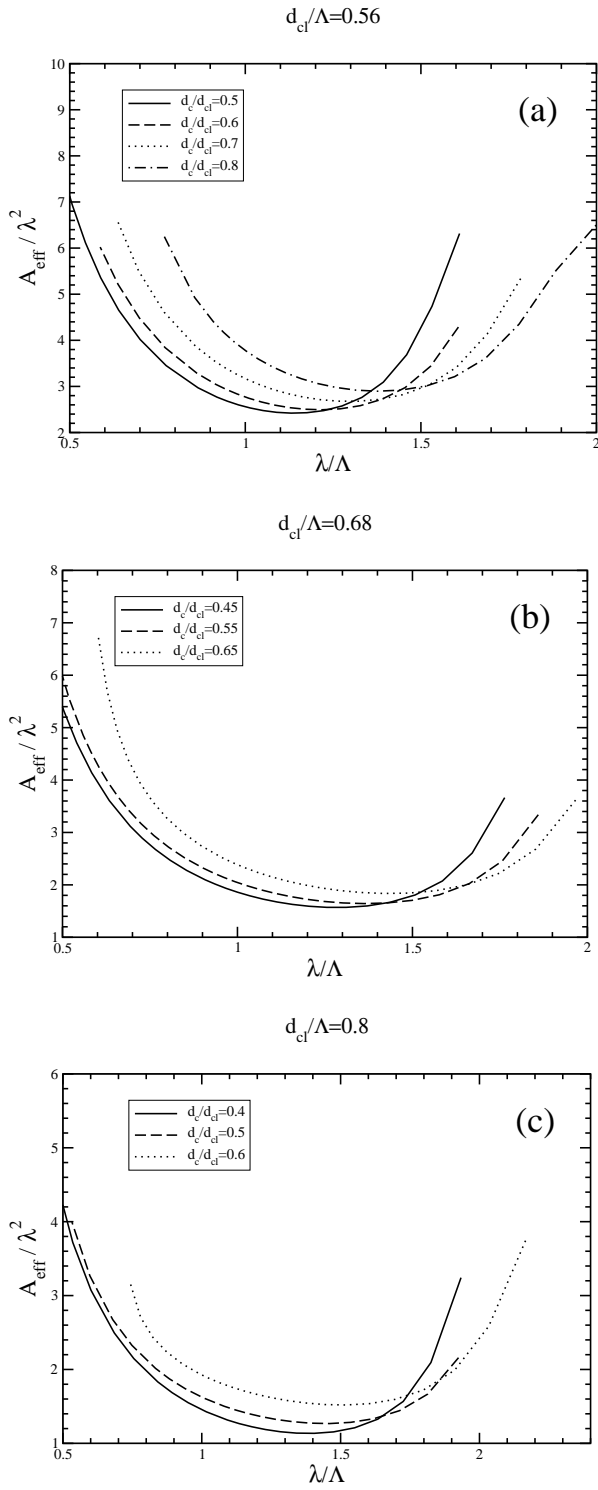


Fig. 4. LÆGSGAARD

$d/\Lambda=0.68$

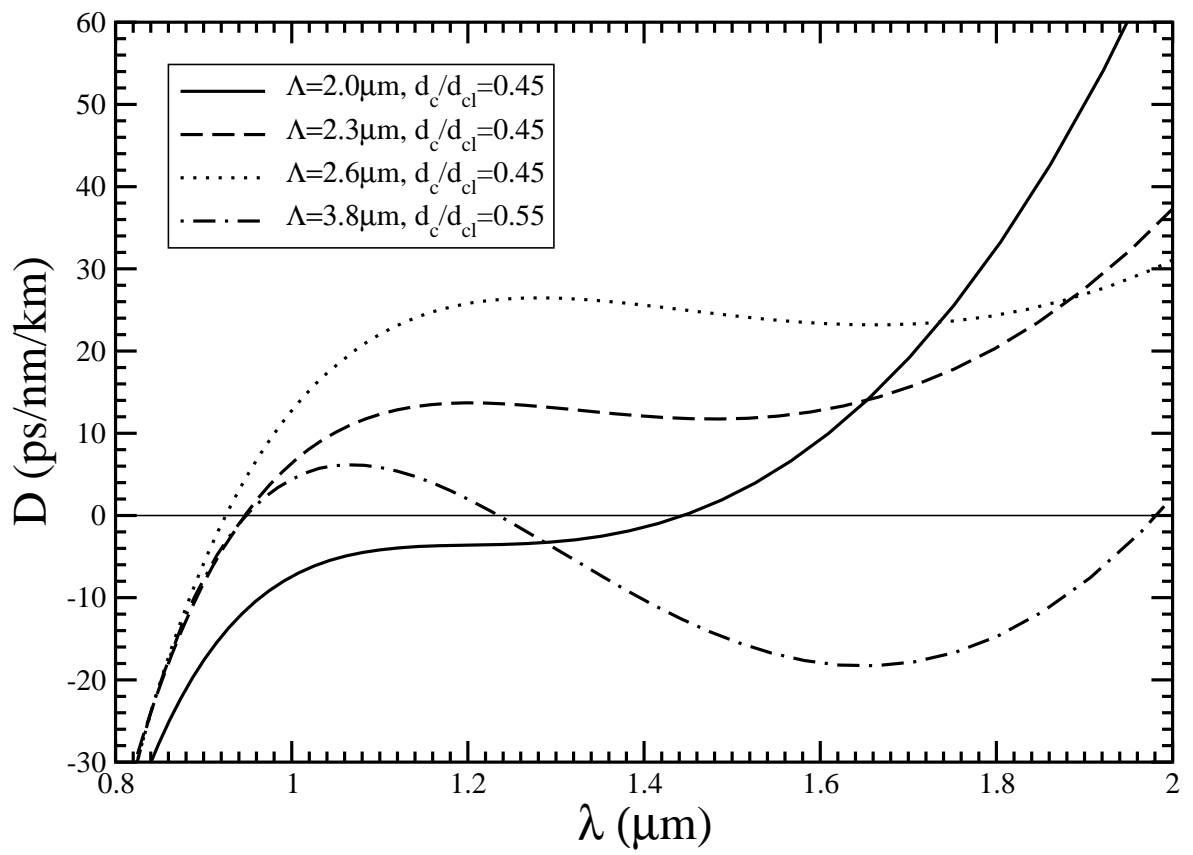


Fig. 5. LÆGSGAARD

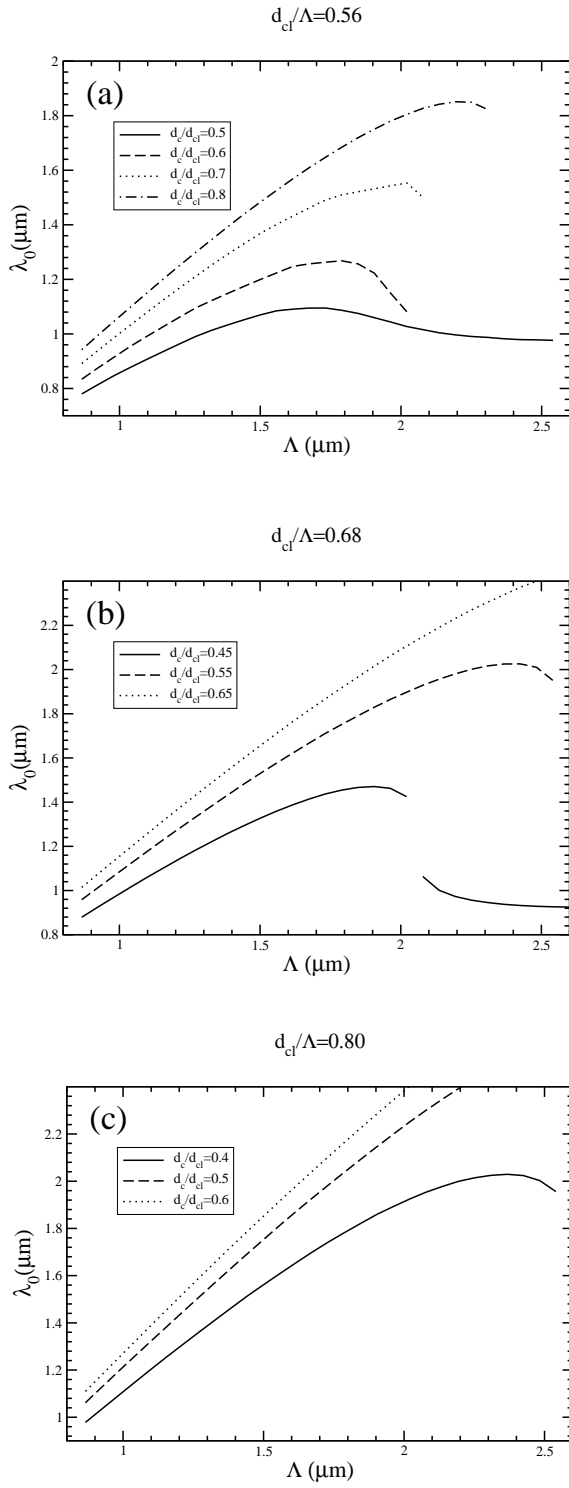


Fig. 6. LÆGSGAARD

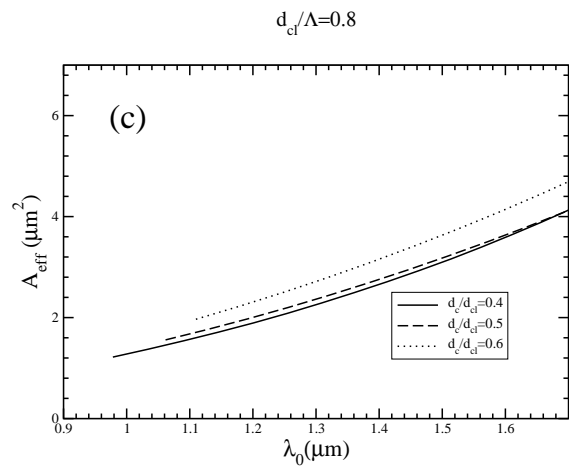
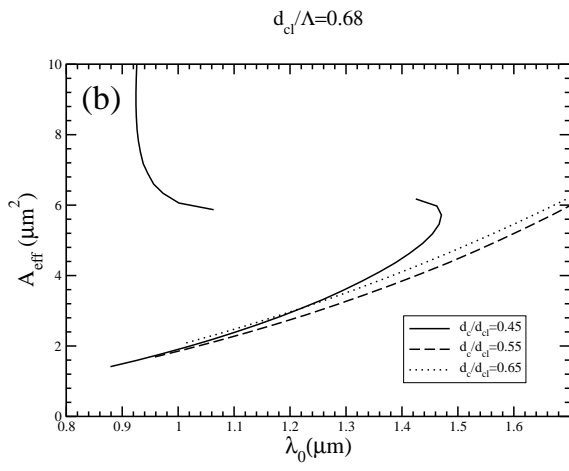
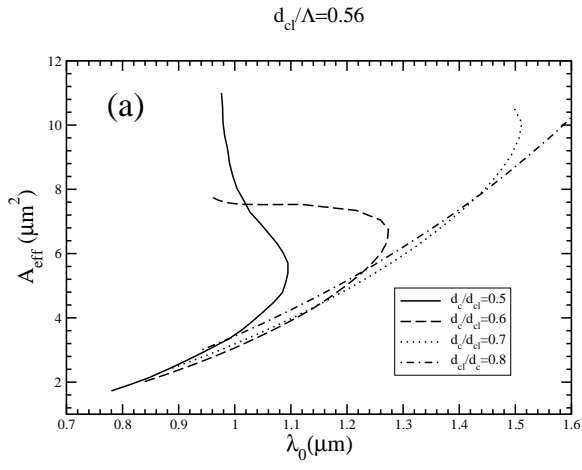


Fig. 7. LÆGSGAARD

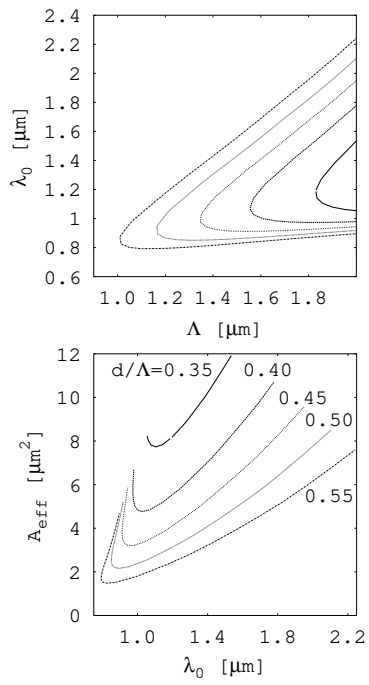


Fig. 8. LÆGSGAARD

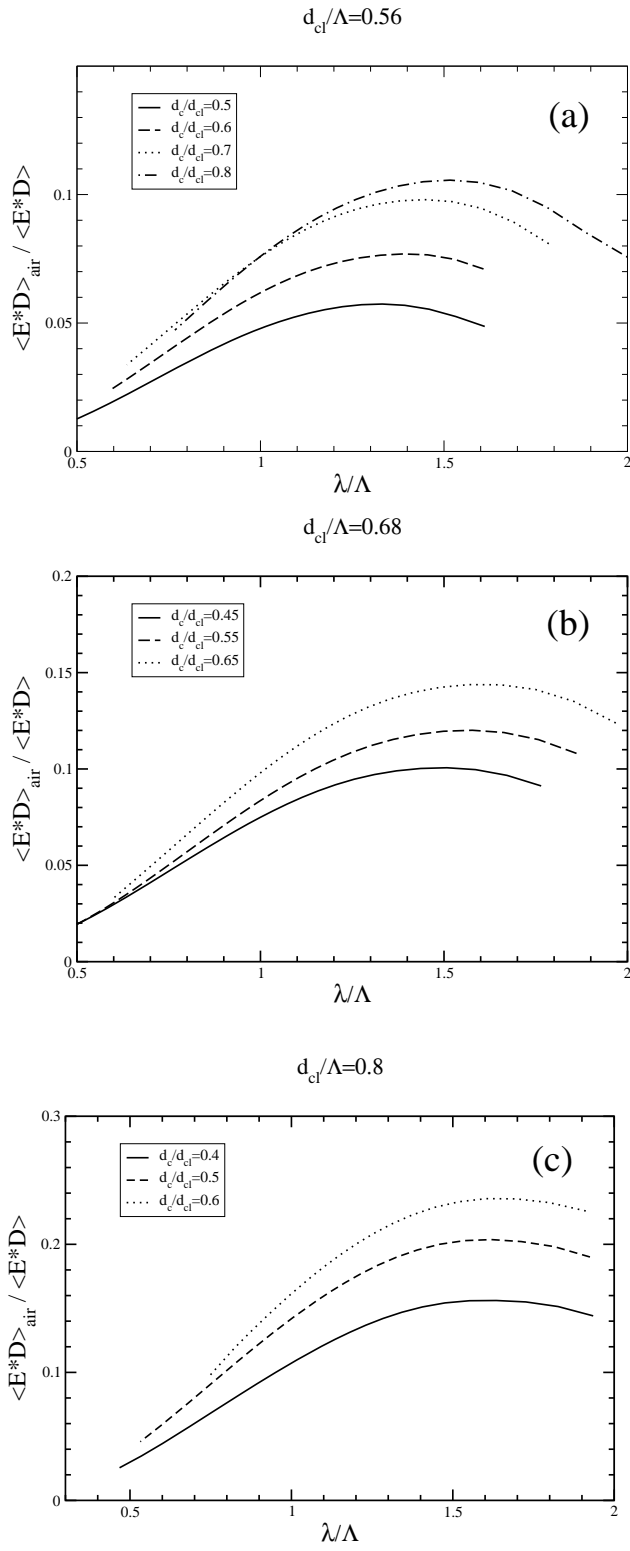


Fig. 9. LÆGSGAARD

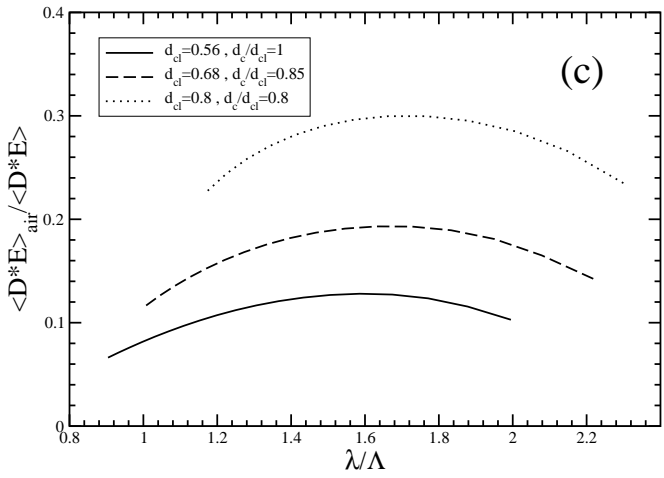
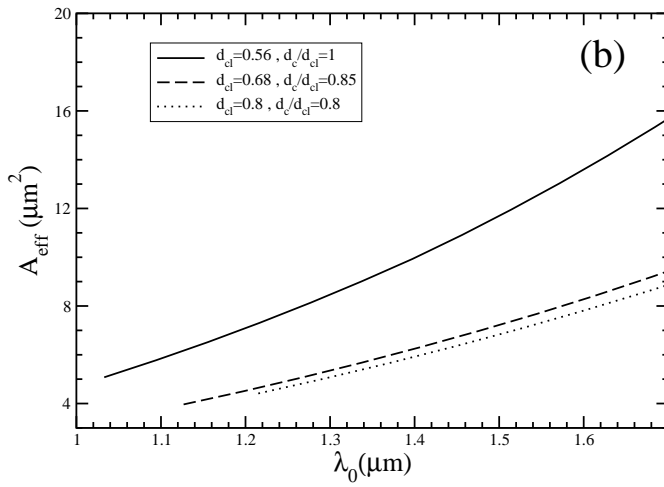
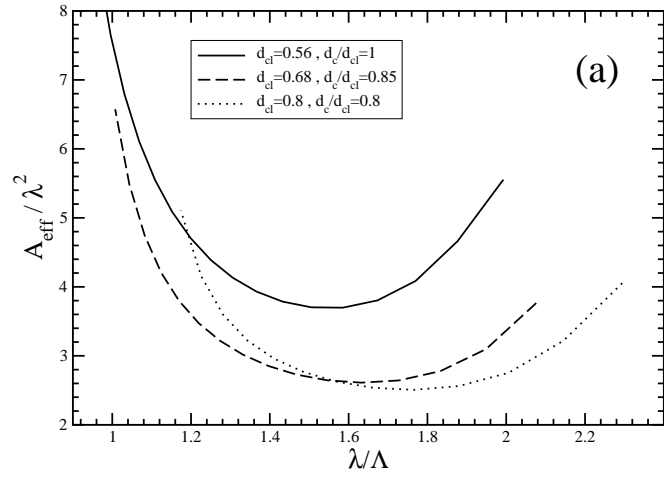


Fig. 10. LÆGSGAARD

$$d_{cl}/\Lambda=0.8$$

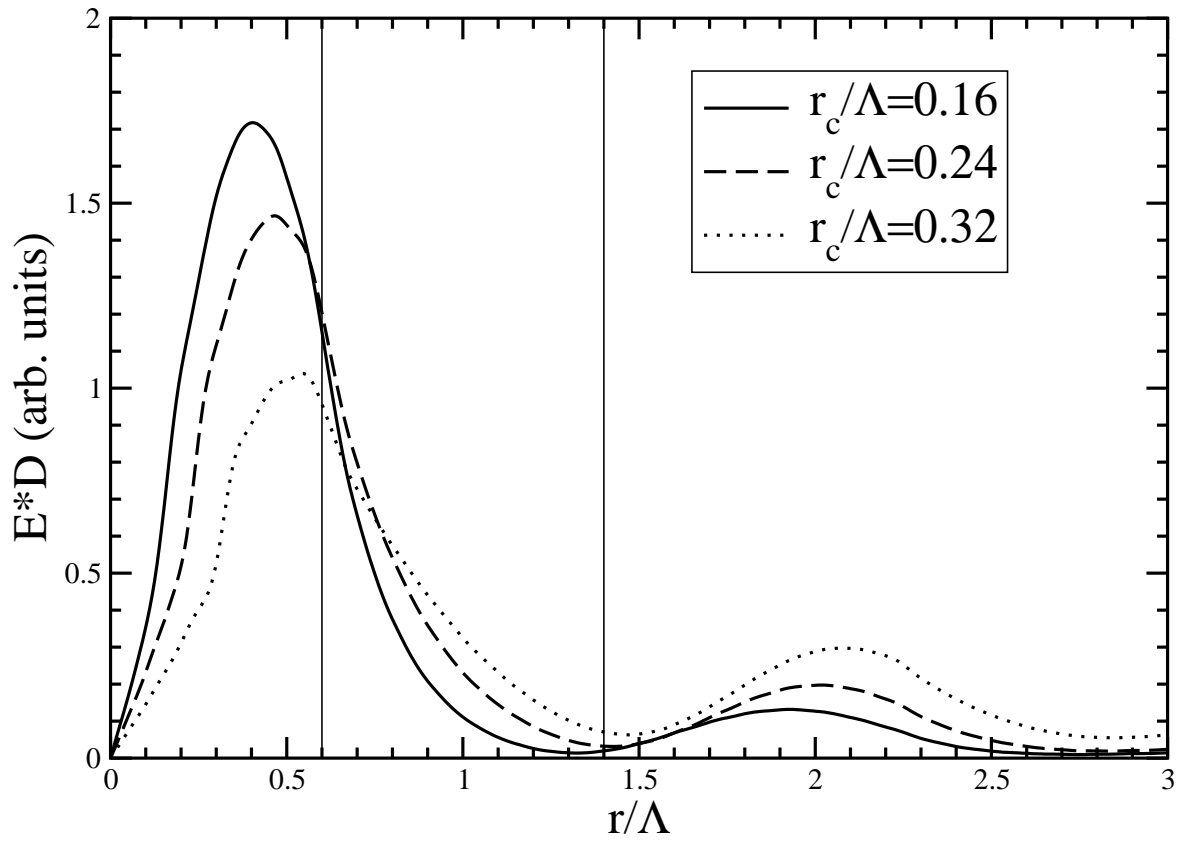


Fig. 11. LÆGSGAARD

$d_{cl}/\Lambda=0.8$

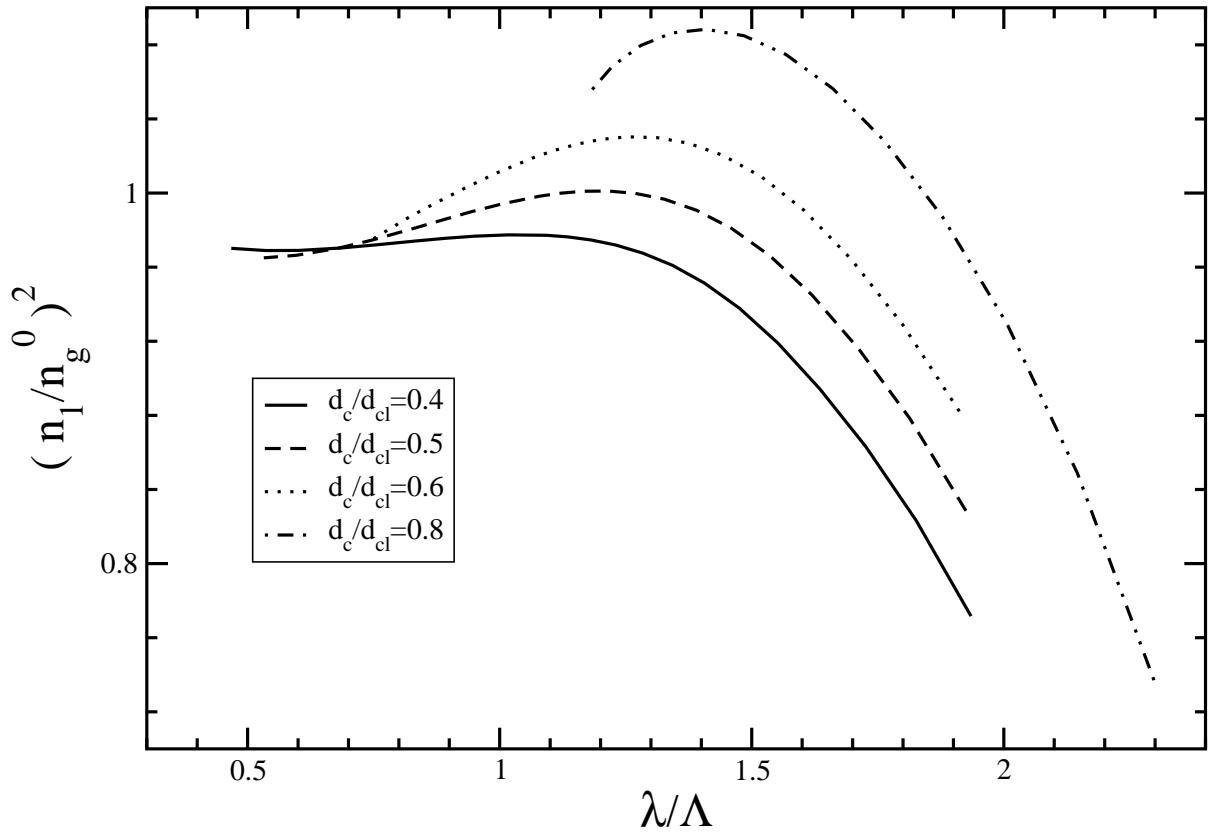


Fig. 12. LÆGSGAARD

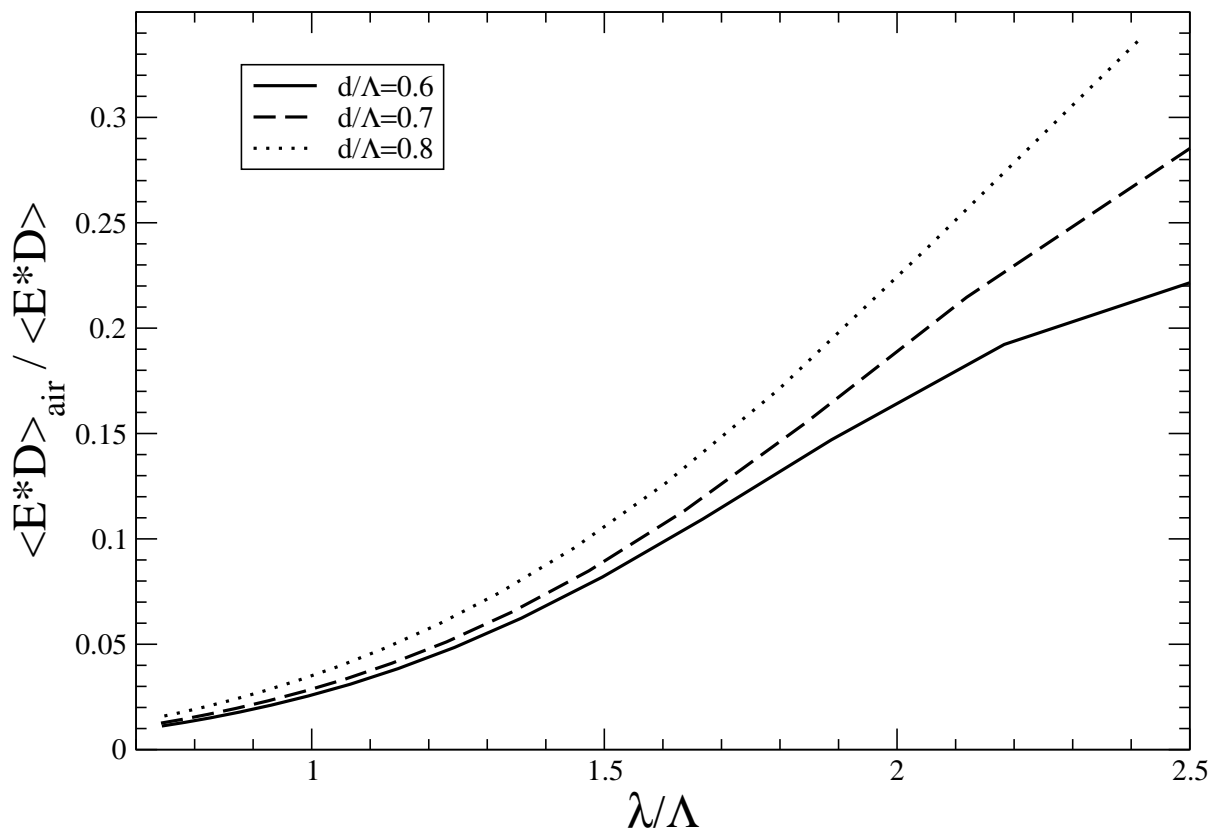


Fig. 13. LÆGSGAARD